RSC Advances

ROYAL SOCIETY OF CHEMISTRY

www.rsc.org/advances

Microwave-assisted synthesis of monoclinic-tetragonal $BiVO_4$ heterojunctions with enhanced visible-light-driven photocatalytic degradation of tetracycline

Ming Yan[a], *Yan Yan*[b], *Yilin Wu*[b], *Yinqun Hua*[a], *Weidong Shi*[b,*]

[a] *School of Material Science and Engineering, Jiangsu University, Zhenjiang 212013, China*

[b] *School of Chemistry and Chemical Engineering, Jiangsu University, Zhenjiang 212013, China*

*Corresponding Author**

E-mail: shiweidong321123@163.com

Telephone Number: +86-511-88791800; fax: +86 0511-88791800

ABSTRACT: Recently, the controlled synthesis of semiconductor photocatalyst has received much attention in the field of pollutant degradation. In this study, different crystalline phases of $BiVO_4$ photocatalysts (monoclinic scheelite (M-phase), tetragonal zircon (T-phase) and monoclinic-tetragonal heterojunction (M-T)) had been successfully synthesized via a facile microwave-assisted method. The crystalline phases of products were controlled by switching the organic additives. The photocatalytic activities of the as-prepared samples were evaluated by the degradation of tetracycline (TC) under visible light irradiation. The obtained results clearly showed that the M-T $BiVO_4$ exhibited the highest photodegradation ratio of 80.5% in 1 h among the three samples, which can be attributed to the heterojunction structures between different phases.

Key words: *$BiVO_4$; heterojunction; microwave-assisted method; tetracycline*

1. Introduction

Tetracycline (TC) is a very noted broad-spectrum antibacterial agent widely applied in bacterial infection treatment, which is often found immensely in aquatic circumstance and poses serious threats to the ecosystem and human health by causing proliferation of bacterial drug resistance [1]. Therefore, the elimination of TC from aqueous environments has become a forcible environmental problem. However, the traditional treatments are often constrained by the low efficiency and high cost. Recently, the photocatalytic oxidation has been established to be a promising technique for environmental remediation [2-3] and provide an efficiency tool for the degradation of TC [4-8]. In a view of energy conversion, visible light counts for more than 43% of the incoming solar energy. Thus, to develop the high efficiency visible-light-driven material for photocatalytic degradation of TC is significant but still a challenge [9].

Recent researches in terms of heterogeneous photocatalysis system were tended to focus on the development of new alternatives of the conventional UV-driven TiO_2 to utilize visible light [10]. Bismuth vanadate ($BiVO_4$), as a ternary oxide semiconductor with narrow band gap, has been found to be a promising photocatalyst with high stability, nontoxicity, and visible-light response for applications both in oxygen evolution from water splitting [11-14] and environmental remediation [15-18]. As we all known, the $BiVO_4$ has three crystalline types: monoclinic scheelite (M-phase), tetragonal zircon (T-phase) and tetragonal scheelite [19]. However, previous research indicated that the M-phase $BiVO_4$ exhibited higher photocatalytic activity than other phases [20]. Unfortunately, the efficiency of single-phase $BiVO_4$ is still limited by the fast recombination of the photo-induced charge carriers [21].

Over the past years, the construction of the heterojunction structure is a very efficient method to overcome this defect [22-26] by realizing the interfacial charge transfer between phases to inhibit the inside recombination of photogenerated electrons and holes [27-29]. For example, researchers have reported the synthesis of V_2O_5-$BiVO_4$ heterostructure and found that the coupled semiconductor photocatalyst exhibited higher photoactivity degradation of methylene blue (MB) than that of pure $BiVO_4$ under visible light illumination [30]. Moreover, the BiOCl-$BiVO_4$ heterojuction photocatalyst was also reported [31] and showed the increased activity by improving the separation of charge carrier. Very recently, the construction of the heterojuction structure by

different type of crystalline phases of $BiVO_4$ have drawn much attention [32]. Unlike the heterojunction of $BiVO_4$ with other semiconductors, heterojunctions between phases often possess a higher inter-facial or inter-particle charge transfer rate and can be easily obtained by simply adjusting the pH of substrate or the heating temperature in crystallization process [33-34]. Therefore, it is reasonable to expect the high TC degradation efficiency of M-T $BiVO_4$ heterojunction photocatalysts.

More recently, microwave-assisted method has been developed to be a very facile method for the synthesis of tailor-made inorganic materials [35-38]. Compared with other traditional heating methods, microwave irradiation can heat the substrate quickly and uniformly with a plastic (Teflon) reaction container, and thusly obtain a more homogeneous nucleation process and shorter crystallization time, which is very favorable to the synthesis of high efficiency M-T $BiVO_4$ heterojunction photocatalyst.

Herein, we reported the efficient visible-light-driven TC degradation on the M-T $BiVO_4$ heterojunction photocatalyst which was synthesized by microwave-assisted method. It should be pointed that the crystalline phases of $BiVO_4$ were controlled by only switching the employed organic additives. In addition, the M-T $BiVO_4$ showed the highest TC degradation activity than the other samples. Furthermore, tentative mechanism of the enhanced photocatalytic activities was also discussed in this paper.

2. Experimental Section

2.1. Chemicals

Bismuth nitrate, ammonium metavanadate and tetracycline were purchased from Aladdin (China). The rest of reagents were all purchased from Sinopharm (China). All reagents were of analytical grade without further purification and the deionized water was used in all experiments.

2.2. Synthesis

The $BiVO_4$ photocatalyst was obtained by a simple microwave-assisted method. A typical synthesis preparation was as follows: 1 mmol $Bi(NO_3)_3 \cdot 5H_2O$ was dissolved into 15 ml deionized water to make a hydrolyzed white floccule suspension. 1 mmol NH_4VO_3 was dissolved in 20 ml of distilled water and then heated at about 70 ^oC with stirring for 10 min to produce a clear solution. Then these two solutions were mixed together to form the light yellow solution under vigorous stirring. After stirring for 30 min, 0.2 g EDTA or 0.4 g EDTA-Na_2 was added into

the above light yellow solution and stirred for another 30 min. The obtained mixture was transferred into a plastic (Teflon) reaction container. The microwave reaction was carried out into a microwave reactor (MDS-6, Xinyi microwave Chemical Company) with the operating power of 1000W and working temperature of 100 ^{o}C for 1 h. After the container cooled down to the room temperature, the precipitates were collected by centrifugation, washed with the deionized water and absolute ethanol three times, dried at 60 ^{o}C for 12 h. At last, the obtained samples were T-phase, M-phase and M-T samples, in which the M-T sample was prepared by 1h with noting, the M-phase sample was obtained by 1h with 0.2g EDTA and the T-phase sample was formed by 1h with 0.4g EDTA-Na_2.

2.3. Characterization

The crystalline phases of the as-synthesized samples were determined by X-ray diffraction (XRD) patterns using a D/MAX-2500 diffract meter (Rigaku, Japan) with a Cu Kα radiation source (λ = 1.54056 Å) at a scan rate of 5 ° min^{-1}. The applied current was 300 mA and the accelerating voltage was 50 kV. The morphologies of the samples were obtained by scanning electron microscopy (SEM) which the images were collected on an S-4800 field emission SEM (FESEM, Hitachi, Japan). Transmission electron microscopy (TEM) and high-resolution transmission electron microscopy (HRTEM) were gathered on an F20 S-TWIN electron microscope (Tecnai G2, FEI Co.) with a 200 kV accelerating voltage. The UV-vis absorption spectra were recorded on a UV 2550 (Shimadzu, Japan) UV-vis spectrophotometer. $BaSO_4$ was used as a reflectance standard. Steady state luminescence experiments were performed using a Photon Technology International Model Quantamaster-QM4m spectrofluorimeter equipped with a 75 W lamp and dual excitation monochromators.

2.4. Photocatalytic activity

Photocatalytic activities of the as-prepared samples were determined by the photodegradation of TC solution which were carried out at 308 K in a photochemical reactor under visible light irradiation. The as-prepared $BiVO_4$ (0.1 g) was mixed with the TC solution (0.1 L, 10 mg/L), followed by magnetic stirring in darkness for 30 min to reach an adsorption equilibrium. The photochemical reactor was irradiated with a 150 W xenon lamp which was located with a distance of 8 cm at one side of the containing solution. UV light with a wavelength less than 420 nm was removed by a UV-cutoff filter. In 10 min irradiation intervals, a series of aqueous solution samples

(6 ml) were collected and separated from the suspended catalyst particles for analysis. The photocatalytic degradation ratio (DR) was calculated via the following formula:

$$DR = (1- A_i / A_0) \times 100\% \quad (1)$$

where A_0 is the foremost absorbency of TC that arrived adsorption equilibrium, A_i is the absorbency after the sampling analysis. The TC concentration of different samples were measured on a UV-vis spectrophotometer by monitoring its characteristic absorption wavelength at 357 nm.

3. Results and discussion

3.1. Morphology and structure

Three $BiVO_4$ materials with different crystalline phases were obtained by developing the microwave-assisted method and different reaction conditions, namely T-phase sample, M-phase sample and M-T sample. Fig. 1 displays the XRD patterns of different $BiVO_4$ samples. All peaks of the T-phase sample in the XRD pattern can be well indexed into tetragonal zircon phase (JCPDS no.14-0133), while the peaks of the M-phase sample are indexed into the monoclinic scheelite phase (JCPDS no.14-0688). M-T sample has XRD patterns with both M-phase and T-phase peaks, which demonstrates the binary compositions of M-T $BiVO_4$ sample. The crystalline structures of different samples were adjusted by only change the additive reagents during the synthesis process.

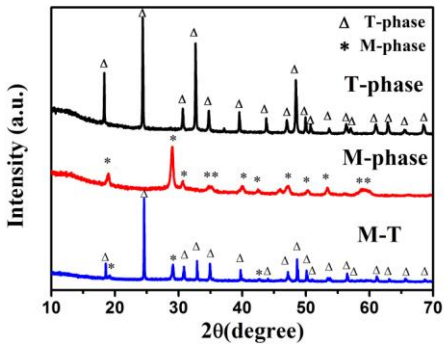

Fig. 1. XRD patterns of T-phase sample, M-phase sample and M-T sample.

Fig. 2 shows SEM images of the different samples. As described in Fig. 2a and b, the M-T sample exhibits the rod-like structure with nanoparticles scattering on the surface. The rod-like structures have a length of 3 - 5μm while the scattering nanoparticles have diameters of about 100

nm. From the Fig. 2c and d, the M-phase sample exhibits massive 2D sheet structure with an average thickness of 30 nm. Fig. 2e and f show that the T-phase sample exhibite spherical structure in micro-scale with rough surface. The diameter of T-phase microspheres is about 2.5μm. SEM studies indicate that the changing additives can also control the morphology of $BiVO_4$ as well as the crystalline structure.

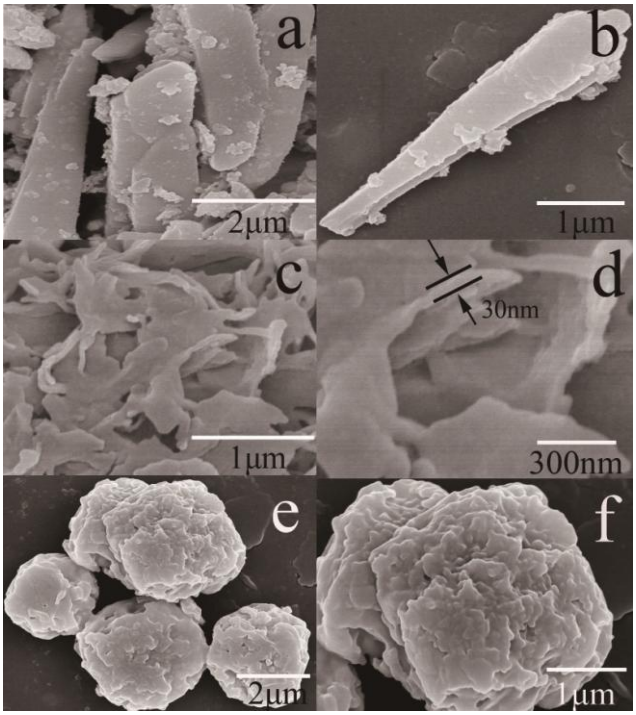

Fig. 2. SEM images of M-T sample: (a) and (b), M-phase sample: (c) and (d), T-phase sample: (e) and (f).

Further insight into the morphology and detailed surface nature of the M-T sample was obtained using transmission electron microscopy (TEM) and high-resolution transmission electron microscopy (HRTEM). As shown in Fig. 3a, the rod structure and scattering nanocrystals of the M-T sample can be easily recognized. From HRTEM image (Fig. 3b) of an individual micro-rod surface, distinct lattice fringes with spacing of d=0.365 nm for rod structure and d=0.312 nm for surface nanocrystal can be observed, which coincide with the (200) plane of T-phase and the (-130) plane of M-phase of $BiVO_4$, respectively. The above obtained results clearly demonstrate the inter-facial (or inter-particle) junction between M-phase and T-phase crystalline phases of $BiVO_4$ have been formed.

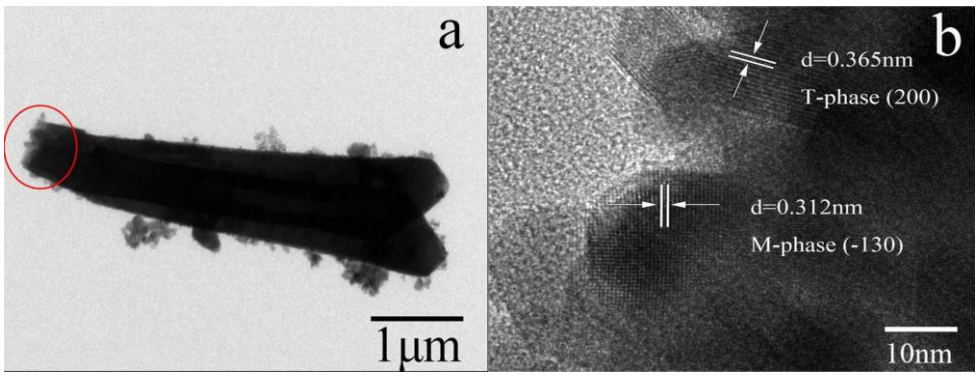

Fig. 3. TEM (a) and HRTEM (b) images of M-T sample.

To figure out the crystallization process of M-T $BiVO_4$, a series of time-resolved experiments were carried out. In these experiments, only the reaction time was changed without altering any other reaction conditions. Fig. 4 shows the SEM images and the corresponding XRD patterns of the obtained samples at different reaction times (from 1min, 15min, 30min and 45min). From which, we envision that both the morphologies and crystalline structures changed during the microwave heating. At the early stage of crystallization with only a very short time (1min) of heating, M-phase $BiVO_4$ can be recognized in the XRD pattern even T-phase is predominant. With continuously heating, M-phase $BiVO_4$ was enhanced (Fig. 4e) with the morphology of sample changed from amorphous nanoparticle to micro-rod structure (Fig. 4 a-d).

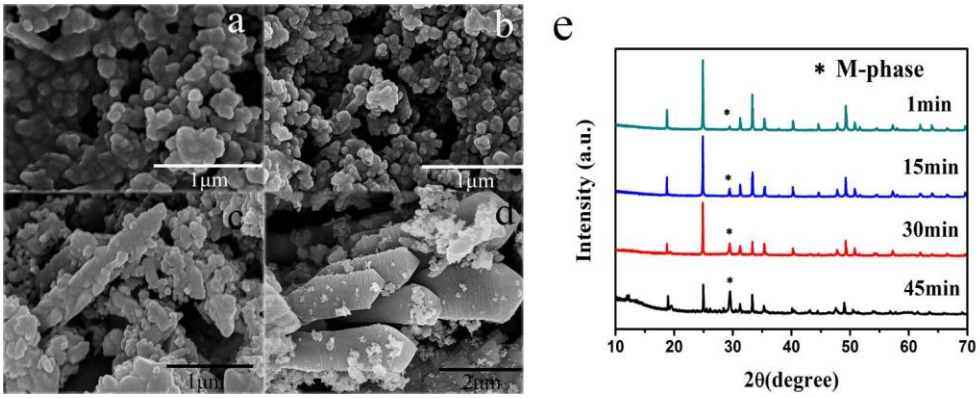

Fig. 4. SEM images of the obtained samples with different microwave reaction times of (a) 1min, (b) 15min, (c) 30min (d) 45min and (e) XRD patterns of M-T $BiVO_4$.

3.2. UV-vis absorption spectra and specific surface area

The light harvesting abilities of different $BiVO_4$ samples were measured by UV-vis absorption spectroscopy. From the Fig. 5a, all the samples exhibit excellent visible-light absorption ability. Among them, the T-phase sample shows weaker light absorption ability than the M-phase sample

and the M-T sample with the light absorption edge at 510 nm. The M-phase sample has absorption edge at 550 nm, while the M-T sample has the light absorption edge at 560 nm. Energy band gaps (Eg) of different samples were also estimated by the following equation [39]:

$$\alpha = A\,(h\nu - Eg)^{n/2} / h\nu \qquad (2)$$

where α, h, *ν*, A, Eg are the absorption coefficient, Planck's constant, the incident light frequency, constant and the band gap energy, respectively. Among them, n depends on the characteristics of the optical transition of the semiconductor, n=1 for direct transition semiconductors and n=4 for indirect transition semiconductors. $BiVO_4$ is a typical kind of direct transition semiconductors and the value of n is chosen to be 1 [40-42]. The estimated band gaps from the plots of $(\alpha h\nu)^2$ versus h*ν* are shown in Fig. 5b, from which, energy band gaps of T-phase, M-phase and M-T samples are 2.75, 2.4 and 2.3, respectively.

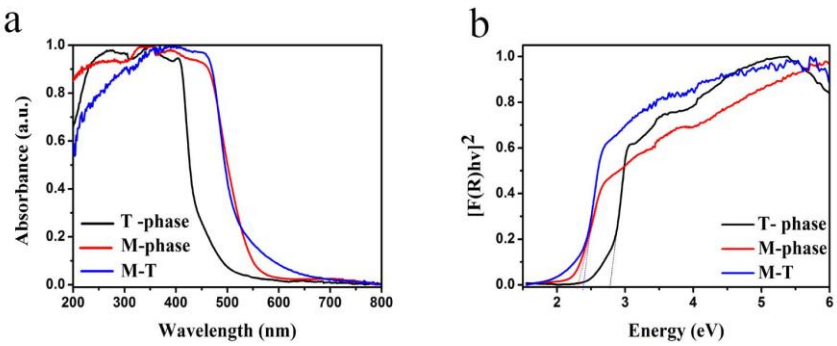

Fig. 5. (a) UV-vis adsorption spectra, (b) calculated band gap of T-phase sample, M-phase sample and M-T sample.

The nitrogen adsorption-desorption isotherm and BET surface areas of the as-prepared samples are displayed in the Fig. 6. From the picture, it can be clearly observed that the BET surface areas of the T-phase sample, M-phase sample and M-T sample are 2.81m^2/g, 3.08m^2/g and 5.15m^2/g, respectively. Moreover, it is known that the photocatalytic activity highly depends on the specific surface areas, the larger surface area of $BiVO_4$ samples can facilitate to adsorb more TC molecules, which are benefit for improving their visible light activities.

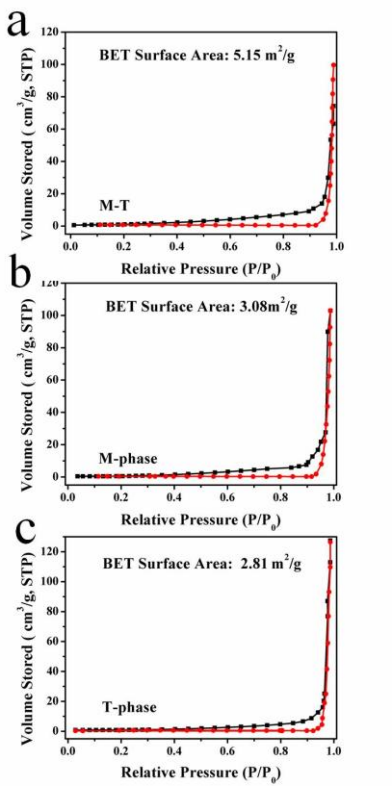

Fig. 6. Nitrogen adsorption-desorption isotherm and BET surface areas of the T-phase, M-phase and M-T samples.

3.3. Photocatalytic degradation of TC

The photocatalytic activities of different $BiVO_4$ samples and commercial Degussa P25 TiO_2 powder were evaluated by the degradation of TC under visible-light irradiation. In order to make a comparison, blank experiment was also conducted without catalyst and little decrease of TC concentration can be observed. As shown in the Fig. 7, the degradation ratio over P25 was14.5%, indicating that the activity with regard to the TC degradation is very poor. However, the M-T sample exhibits the high activity with the degradation ratio of 80.5%, which is much higher than the M-phase sample and the T-phase sample for 60.2% and 17.3%, respectively. In addition, the time-resolved TC absorption spectra with the M-T sample under visible light irradiation is displayed in the Fig. 8. From which, the intensity of the TC absorption peaks at 357 nm is gradually decreased. Many studies have pointed out that the photocatalytic activity of $BiVO_4$ has a close relationship with the crystal structure [33-34]. In this work, we also found the M-T $BiVO_4$ sample showed higher photocatalytic activity than both M-phase and T-phase samples, which can be attributed to the heterojunction structures between M-phase and T-phase that facilitated the

charge transfer between phases to inhibit the recombination of photo-induced charge carriers. In order to exam the credibility of our results of photodegradation ratio, the dark experiments was carried out to removed the effect of physical adsorption in the Fig. 9. Within 20min, all the samples arrive adsorption equilibrium, suggesting that the effect of the physical adsorption was removed and the activity of the as-prepared samples were correctly evaluated.

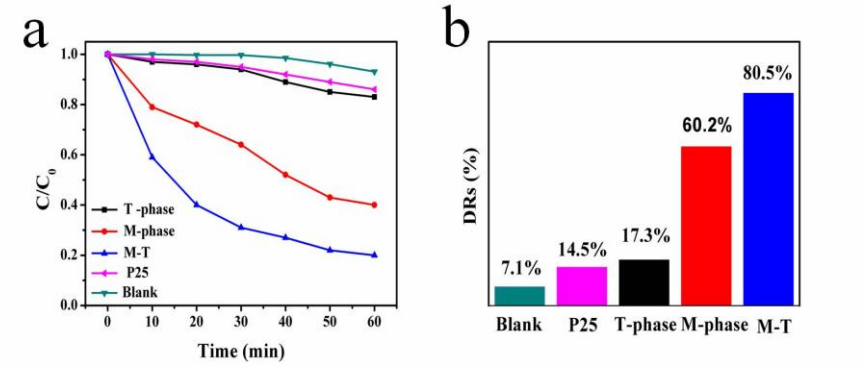

Fig. 7. Photocatalytic degradation of TC versus visible light irradiation time with different samples.

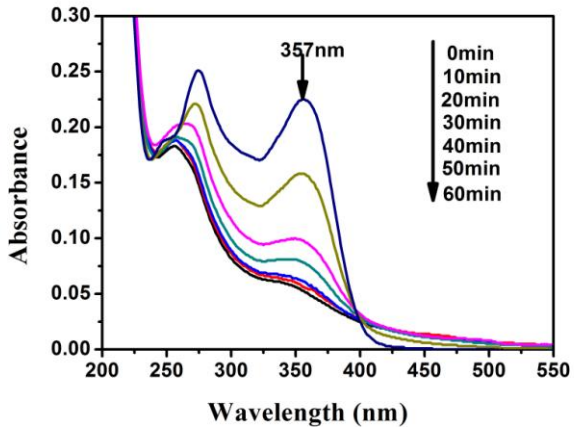

Fig. 8.Time-dependent UV-vis absorption spectra of the TC solution in the presence of M-T sample.

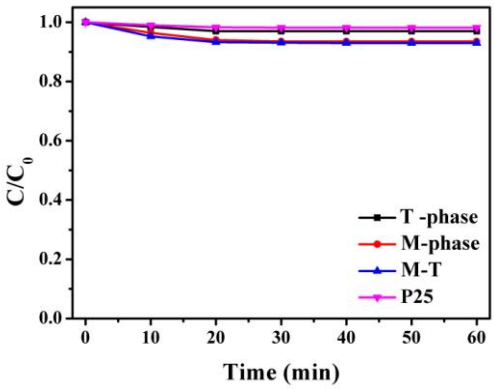

Fig. 9. Adsorption equilibrium curves of different samples in 60 min kept in darkness.

The kinetics study was employed to further illustrate the photocatalytic activities in Fig. 10. The kinetic rate constants were gained by a Langmuir-Hinshelwood model and the decomposition of TC matched the first order kinetic equation:

$$\ln(C_0/C) = k_{app}\, t \qquad (3)$$

where C and C_0 represent the TC concentration remaining in the solution at irradiation time of t and the initial concentration at t =0, respectively. k_{app} expresses the constant of degradation rate. The k_{app} values are 0.00321, 0.01532, 0.02569 and 0.00249 for T-phase, M-phase M-T and P25 samples. Obviously, the k_{app} value of the M-T sample (0.02569) is the highest among all the samples, which is consistent with the conclusion of photocatalytic degradation.

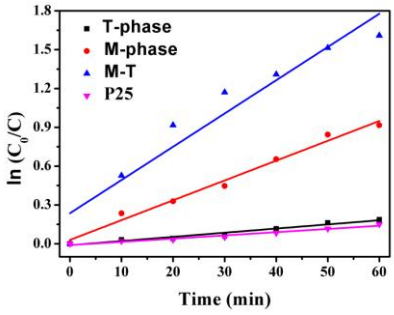

Fig. 10. Kinetics of the photocatalytic degradation ratio with the different samples.

3.4. Investigation of reactive species

As is well-known, many reactive species such as h^+, $\bullet O_2^-$, and $\bullet$OH play major roles on TC decomposed [43-44]. In our work, $\bullet O_2^-$ could not be produced because of more positive

reduction potential of -0.33eV/NHE (O_2/ • O_2^-) by electrons [45], compared to the M-phase (E_{VB}=0.34eV) and T-phase (E_{VB}=0.16eV). However, due to the reduction potential of O_2/H_2O_2 was 0.695eV [43], the electrons can react to generate •OH via the O_2 and H^+ with the equation: $O_2 + 2e^- + 2H^+ = H_2O_2$, $H_2O_2 + e^- = \bullet OH + OH^-$. In comparison to the potential of •OH/OH^- (2.38eV/NHE) and •OH/H_2O (2.72eV/NHE)， the VB of M-phase $BiVO_4$ is 2.74eV, so the •OH could produce with the react of h^+, OH^- and H_2O on the M-T $BiVO_4$ surface. The •OH can just react with TC immediately.

A series of active species trapping experiments were aimed to further investigate the photocatalytic oxidation mechanism of TC degradation by the M-T sample. $AgNO_3$, iso-propanol (IPA) and triethanolamine (TEA) were employed as trapping reagents of photogenerated electrons (e^-), •OH radicals and holes (h^+), respectively (Fig. 11). As the TEA (the scavenger of holes) was added into the reaction system, the DR was significantly declined compared to the reaction in the absence of TEA, indicating that the photogenerated holes were the major oxidative species for the oxidation of TC [45-49]. When the IPA was added into the reaction system to trap •OH, the DR of the TC was slightly decreased to 62.2%, which indicate that the •OH took part in the oxidation reaction [50]. However, when the $AgNO_3$ was used as the scavenger of electrons [45-49], the DR increased rather than decreased, which demonstrate that the scavenger of e^- had less opportunity to join recombination of electron-hole pairs' and produce more holes to take part in reaction process.

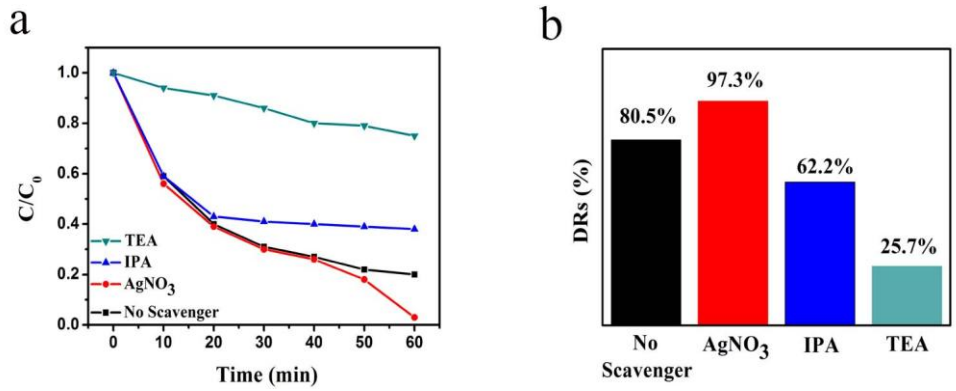

Fig. 11. Photocatalytic degradation ratios of TC using different radical scavengers over M-T sample

3.5 The intermediates of TC degradation

The intermediates of TC were investigated via LC-MS and the results were exhibited in Fig.

12. As shown in Fig. 12a, it can be clearly observed that an intense prominent ion with m/z = 445, which can be attributed to TC. From the analysis of LC-MS, the TC was attacked by the major reactive oxidated species h^+. The successive ions fragmentation during collision-induced dissociation is in the following order: m/z=445→m/z=406 (by loss of OH, H and CH_3)→m/z=362 (by loss of $CONH_{2)}$→m/z=318 (by loss of N, CH_2 and CH_3)→m/z= (then by loss of CH, C, H and OH). On the basis of all the above experimental results and the previous studies [51], the possible processes of the degradation are displayed in Fig. 13. At last, the intermediate products would be degraded to the small inorganic molecular material.

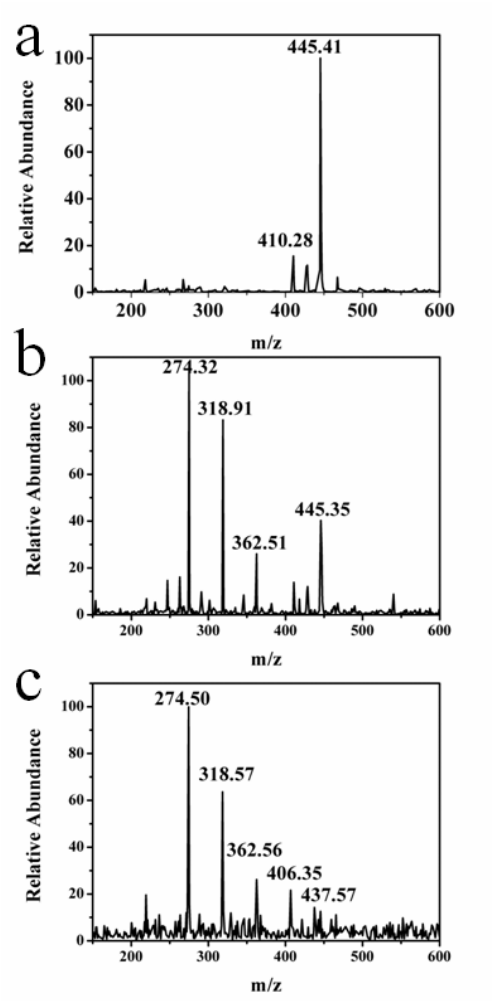

Fig. 12. Typical LC–MS chromatogram at the irradiation for 1h.

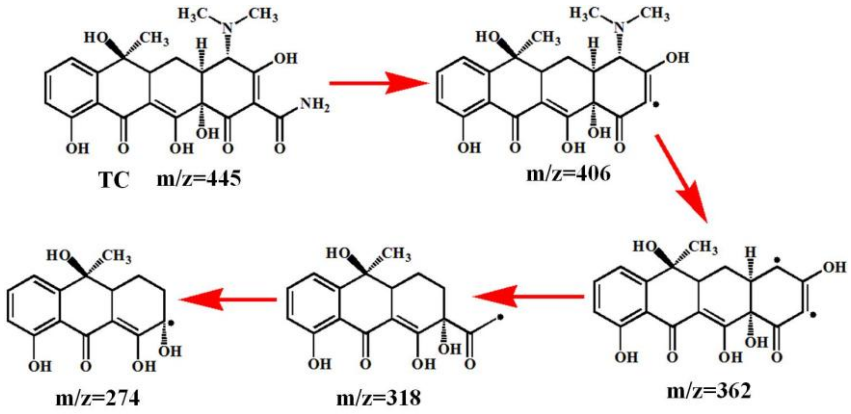

Fig. 13. Proposed degradation pathways for photocatalytic degradation of TC with M-T photocatalyst.

3.6. Possible mechanism of TC degradation by M-T $BiVO_4$

The possible mechanism of the TC degradation by M-T $BiVO_4$ was then discussed in detail. As shown in Fig. 14, T-phase $BiVO_4$ has larger energy band gap than M-phase phase $BiVO_4$ with both higher CB bottom and lower VB top positions. Under visible-light irradiation, both T-phase and M-phase $BiVO_4$ were excited and produced photo-induced electrons and holes on CB and VB. Due to the heterojunction structure between T-phase and M-phase of $BiVO_4$, electrons on T-phase CB can easily injected into the CB of M-phase phase. On the other hand, holes on T-phase VB can also injected into M-phase VB, which effectively inhibit the recombination of electrons and holes, and promote photocatalytic activity [52].

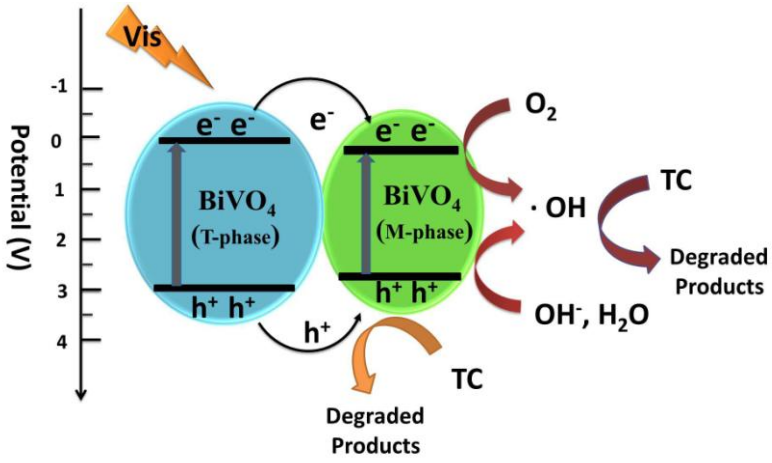

Fig. 14. Photocatalytic mechanistic of M-T $BiVO_4$ heterojunctions under visible light irradiation.

3.7. Photoluminescence spectra analysis

Photoluminescence (PL) analysis was also conducted to evaluate the separation ability of photogenerated charge carriers [53]. The measurement was conducted at the excitation wavelength of 360 nm with a photomultiplier tube voltage of 500 V. From the Fig. 15, all the samples have PL emission peak at 469 nm and the peak intensity of different specific samples were in the order of T-phase sample, M-phase sample and M-T sample, which is the exact reverse order of DR. It is well-acknowledged that the PL emission intensity of a semiconductor is proportional to the opportunity for the recombination of photoinduced electron-hole pairs [54]. In other words, the lower PL intensity implies the stronger charge-separation ability. The completely opposite PL and DR data sufficiently demonstrate the validity of our assumption.

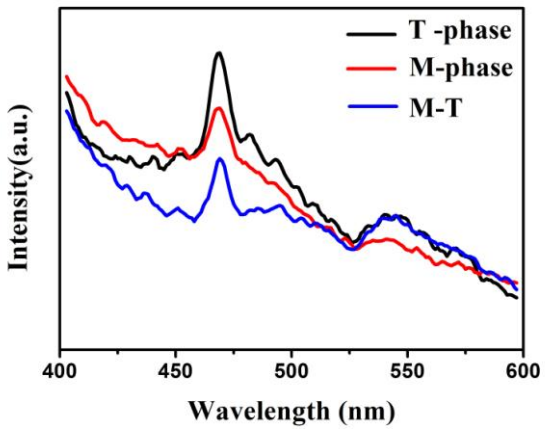

Fig. 15. Photoluminescence spectra of T-phase sample, M-phase sample amd M-T sample.

3.8. Photostability

The stability of the M-T sample was evaluated by the repeating experiments. After each run, the catalysts were collected and washed by simple filtration followed by ultrasonic cleaning with deionized water. As shown in Fig. 16a, the M-T sample exhibite a high stability, resulting in a high decomposition ratio even after four cycles. Meanwhile, the XRD patterns of the M-T sample is barely changed after four cycle experiments (Fig. 16b). In addition, the SEM after four cycles remain unchanged, which is displayed in Fig. S1. These results clearly suggest that the photocatalysts have excellent photostability.

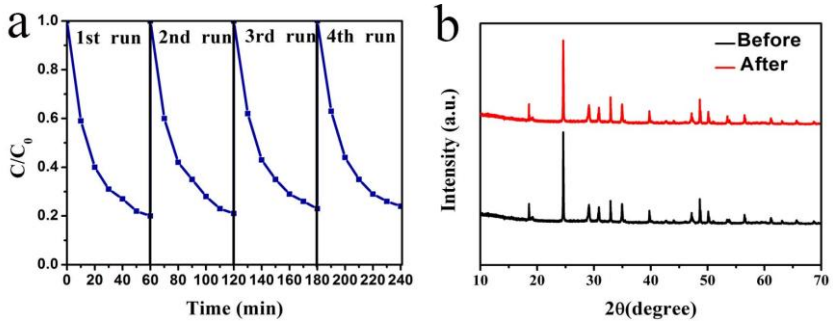

Fig. 16. (a) Four cycle experiments of M-T sample, (b) XRD patterns of the M-T sample before and after four cycle experiments.

4. Conclusions

In summary, different $BiVO_4$ photocatalysts were prepared by the microwave-assisted method. The crystalline phases of products were controlled by varying the organic additives. Visible-light-driven TC degradation was conducted by obtained $BiVO_4$ photocatalysts. Among them, the M-T sample showed the highest DR of 80.5% in 1 h. The high activity of M-T $BiVO_4$ photocatalyst was likely to result from the fast charge transfer between the heterojunction of different phases of $BiVO_4$.

Acknowledgements

The authors greatly gratefully acknowledge the financial support of the National Natural Science Foundation of China (21276116, 21477050, 21301076 and 21303074), Excellent Youth Foundation of Jiangsu Scientific Committee (BK20140011), Chinese-German Cooperation Research Project (GZ1091). Program for High-Level Innovative and Entrepreneurial Talents in Jiangsu Province, Program for New Century Excellent Talents in University (NCET -13-0835), Henry Fok Education Foundation (141068) and Six Talents Peak Project in Jiangsu Province (XCL-025).

References:

[1] M. R. Hoffmann, S. T. Martin, W. Choi, D. W. Bahnemann, Environmental applications of semiconductor photocatalysis, *Chem. Rev,* 1995, 95, 69-96.

[2] C. C. Pei, W. W. Leung, Photocatalytic degradation of Rhodamine B by TiO_2/ZnO nanofibers under visible-light irradiation, *Sep. Purif. Technol*, 2013, 114, 108-116.

[3] Y. Jiang, R. Amal, Selective synthesis of TiO_2-based nanoparticles with highly active surface

sites for gas-phase photocatalytic oxidation, *Appl. Catal. B.*, 2013138-139, 260-267.

[4] Y. B. Liu, X. J. Gan, B. X. Zhou, B. T. Xiong, J. H. Li, C. P. Dong, J. Bai, W. M. Cai, Photoelectrocatalytic degradation of tetracycline by highly effective TiO_2 nanopore arrays electrode, *J. Hazard. Mater*, 2009, 171, 678-683.

[5] R. A. Palominos, M. A. Mondaca, A. Giraldo, G. Penuela, M. Perez-Moya, H. D. Mansilla, Photocatalytic oxidation of the antibiotic tetracycline on TiO_2 and ZnO suspensions, *Catal. Today*, 2009, 144, 100-105.

[6] C. Reyes, J. Fernandez, J. Freer, M. A. Mondaca, C. Zaror, S. Malato, H. D. Mansilla, Degradation and inactivation of tetracycline by TiO_2 photocatalysis, *J. Photochem. Photobiol. A*, 2006, 184, 141-146.

[7] J. Jeong, W. Song, W. J. Cooper, J. Jung, J. Greaves, Degradation of tetracycline antibiotics: Mechanisms and kinetic studies for advanced oxidation/reduction processes, *Chemosphere*, 2010, 78, 533-540.

[8] J. Huang, L. Xiao, X. Yang, WO_3 nanoplates, hierarchical flower-like assemblies and their photocatalytic properties, *Mater. Res. Bull*, 2013, 48, 2782-2785.

[9] P. W. Huo, Z. Y. Lu, X. L. Liu, X. Gao, J. M. Pan, D. Wu, J. Ying, H. M. Li, Y. S. Yan, Preparation molecular/ions imprinted photocatalysts of La^{3+}@POPD/TiO_2/Fly-Ash ceno-spheres: preferential photodegradation of TCs antibiotics, *Chem.Eng. J.*, 2012, 198-199, 73-80.

[10] A. Kubacka, M. Fernández-García, G. Colón, Nanoarchitectures for solar photocatalytic applications, *Chem. Rev.*, 2012, 112, 1555-1614.

[11] S. Tokunaga, H. Kato, A. Kudo, Selective preparation of monoclinic and tetragonal $BiVO_4$ with scheelite structure and their photocatalytic properties, *Chemistry of Materials*, 2001, 13, 4624-4628.

[12] K. Sayama, A. Nomura, T. Arai, Photoelectrochemical decomposition of water into H_2 and O_2 on porous $BiVO_4$ thin-film electrodes under visible light and significant effect of Ag ion

treatment, *Journal of Physics and Chemistry B*, 2006, 110, 11352-11360.

[13] A. Kudo, K. Omori, H. Kato, A novel aqueous process for preparation of crystal form-controlled and highly crystalline $BiVO_4$ powder from layered vanadates at room temperature and its photocatalytic and photophysical properties, *J. Am. Chem. Soc.*, 1999, 121, 11459-11467.

[14] J. Z. Su, L. J. Guo, S. Yoriya, Aqueous growth of pyramidal-shaped $BiVO_4$ nanowire arrays and structural characterization: application to photoelectrochemical water splitting, C*rystal Growth and Design*, 2010, 10, 856-861.

[15] L. Zhang, D. R. Chen, X. L. Jiao, Monoclinic structured $BiVO_4$ nanosheets: hydrothermal preparation, formation mechanism, and coloristic and photocatalytic properties, *Journal of Physical Chemistry B*, 2006, 110, 2668-2673.

[16] W. Z. Yin, W. Z. Wang, L. Zhou, CTAB-assisted synthesis of monoclinic $BiVO_4$ photocatalyst and its highly efficient degradation of organic dye under visible-light irradiation, *J. Hazard. Mater*, 2010, 173, 194-199.

[17] H. Q. Jiang, H. Endo, H. Natori, Fabrication and photoactivities of spherical-shaped $BiVO_4$ photocatalysts through solution combustion synthesis method, *Journal of the European Ceramic Society*, 2008, 28, 2955-2962.

[18] L. Zhou, W. Wang, S. Liu, A sonochemical route to visible-light-driven high-activity $BiVO_4$ photocatalyst, *Journal of Molecular Catalysis A: Chemical*, 2006, 252, 120-124.

[19] A. Mart ńez-de la Cruz, U. M. García-Pérez, S. Sepúlveda-Guzmán, Characterization of the visible-light-driven $BiVO_4$ photocatalyst synthesized via a polymer-assisted hydrothermal method, *Res. Chem. Intermed*, 2012, 39, 881-894.

[20] S. J. Hong, S. Lee, J. S. Jang, J. S. Lee, Heterojunction $BiVO_4/WO_3$ electrodes for enhanced photoactivity of water oxidation, *Energy Environ. Sci.*, 2011, 4, 1781-1787.

[21] W. Yao, H. Iwai, J. Ye, Effects of molybdenum substitution on the photocatalytic behavior of $BiVO_4$, *Dalton Trans.*, 2008, 11, 1426-1430.

[22] M. Long, W. Cai, H. Kisch, Visible light induced photoelectro chemical properties of n-$BiVO_4$ and n-$BiVO_4$/p-Co_3O_4. *J. Phys, Chem. C.*, 2008, 112, 548-554.

[23] X. Zhang, Y. Gong, X. Dong, X. Zhang, C. Ma, F. Shi, Fabrication and efficient visible light-induced photocatalytic activity of Bi_2WO_6/$BiVO_4$ heterojunction, *Mater. Chem. Phys*, 2012, 136, 72-476.

[24] H. T. Li, X. D. He, Z. H. Kang, H. Huang,Y. Liu, J. L. Liu, S. Y. Lian, C. Him, A. Tsang, X. B. Yang, S. T. Lee, Water-Soluble Fluorescent Carbon Quantum Dots and Photocatalyst Design, *Angew. Chem. Int. Ed*., 2010, 49, 4430-4434.

[25] X. H. Gao, H. B. Wu, L. X. Zheng, Y. J. Zhong, Y. Hu, X. W. Lou, Formation of Mesoporous Heterostructured $BiVO_4$/Bi_2S_3 Hollow Discoids with Enhanced Photoactivity, *Angew. Chem. Int. Ed.*, 2014, 53, 5917-5921.

[26] C. Eley,T. Li, F. L. Liao, S. M. Fairclough, J. M. Smith, G. Smith, S. C. Edman Tsang, Nanojunction-Mediated Photocatalytic Enhancement in Heterostructured CdS/ZnO, CdSe/ZnO, and CdTe/ZnO Nanocrystals, *Angew. Chem. Int. Ed.*, 2014, 53, 7838-7842.

[27] J. Z. Su, L. J. Guo, N. Z. Bao, C. A. Grimes, Nanostructured WO_3/$BiVO_4$ heterojunction films for efficient photoelectrochemical water splitting, *Nano Letters*. 2011, 11, 1928-1933.

[28] P. Ju, P. Wang, B. Li, H. Fan , S. Y. Ai, D. Zhang, Y. Wang, A novel calcined Bi_2WO_6/$BiVO_4$ heterojunction photocatalyst with highly enhanced photocatalytic activity, *Chem.Eng. J.*, 2013, 236, 430-437.

[29] W. R. Zhao, Y. Wang, Y. Yang, J. Tang, Y. A. Yang, Carbon spheres supported visible-light-driven CuO-$BiVO_4$ heterojunction: Preparation, characterization, and photocatalytic properties, *Appl. Catal. B.*, 2012, 115-116, 90-99.

[30] J. Su, X. X. Zou, G. D. Li, X. Wei, C. Yan, Y. N. Wang, J. Zhao, L. J. Zhou, J. S. Chen, Macroporous V_2O_5/$BiVO_4$ composites: effect of heterojunction on the behavior of photogenerated charges. *J. Phys. Chem. C.*, 2011, 115, 8064-8071.

[31] Z. Q. He, Y. Q. Shi, C. Gao, L. N. Wen, J. M. Chen, S. Song, BiOCl/$BiVO_4$ p−n

heterojunction with enhanced photocatalytic activity under visible-light irradiation, *J. Phys. Chem. C.*, 2014, 118, 389-398.

[32] S. Usai, S. Obregón, A. I. Becerro, G. Colón, Monoclinic−tetragonal heterostructured $BiVO_4$ by yttrium doping with improved photocatalytic activity, *J. Phys. Chem. C.*, 2013, 117, 24479-24484.

[33] H. M. Fan, T. F. Jiang, H. Y. Li, D. J. Wang, L. L. Wang, J. L. Zhai, D. Q. He, P. Wang, T. F. Xie, Effect of $BiVO_4$ crystalline phases on the photoinduced carriers behavior and photocatalytic activity, *J. Phys. Chem. C.*, 2012, 116, 2425-2430.

[34] G. Q. Tan, L. L. Zhang, H. J. Ren, S. S. Wei, J. Huang, A. Xia, Effects of pH on the hierarchical structures and photocatalytic performance of $BiVO_4$ powders prepared via the microwave hydrothermal method, *ACS Appl. Mater. Interfaces*, 2013, 5, 5186-5193.

[35] W. D. Shi, Y. Yan, X. Yan, Microwave-assisted synthesis of nano-scale $BiVO_4$ photocatalysts and theirexcellent visible-light-driven photocatalytic activity for the degradation of ciprofloxacin, *Chem.Eng. J.*, 2013, 215-216, 740-746.

[36] M. Yan, Y. Yan, C. Wang , W. Lu , W. D. Shi, Ni^{2+} doped $InVO_4$ nanocrystals: One-pot microwave-assisted synthesis and enhanced photocatalytic O_2 production activity under visible-light, *Materials Letters*, 2014, 121, 215-218.

[37] Y. Yan, S. F. Sun, Y. Song, X. Yan, W. S. Guan, X. L. Liu, W. D. Shi, Microwave-assisted in situ synthesis of reduced graphene oxide-$BiVO_4$ composite photocatalysts and their enhanced photocatalytic performance for the degradation of ciprofloxacin, *J. Hazard. Mater,* 2013, 250-251, 106-114.

[38] Y. Yan, F. P. Cai, Y. Song, W. D. Shi, $InVO_4$ nanocrystal photocatalysts: Microwave-assisted synthesis and size-dependent activities of hydrogen production from water splitting under visible light, *Chem.Eng. J.*, 2013, 233, 1-7.

[39] M. A. Butler, Photoelectrolysis and physical properties of the semiconducting electrode WO_2, *Journal of Applied Physics*, 1977, 48, 1914-1920.

[40] M. L. Guan, D. K. Ma, S. W. Hu, Y. J. Chen, S. M. Huang, From hollow olive-shaped $BiVO_4$ to n-p core-shell $BiVO_4$@Bi_2O_3 microspheres: controlled synthesis and enhanced visible-light-responsive photocatalytic properties, *Inorganic Chemistry*, 2011, 50, 800-805.

[41] J. Z. Su, L. J. Guo, S. Yoriya, C. A. Grimes, Aqueous growth of pyramidal-shaped $BiVO_4$ nanowire arrays and structural characterization: application to photoelectrochemical water splitting, *Crystal Growth and Design*, 2010, 10, 856-861.

[42] L. Dong, S. Guo, S. Y. Zhu, D. F. Xu, L. L. Zhang, M. X. Huo, X. Yang, Sunlight responsive $BiVO_4$ photocatalyst: effects of pH on L-cysteine-assisted hydrothermal treatment and enhanced degradation of ofloxaci, *Catalysis Communications*, 2011, 16, 250-254.

[43] L. S. Zhang, K. H. Wong, H. Y. Yip, C. Hu, J. C. Yu, C. Y. Chan, P. K. Wong, Effective photocatalytic disinfection of E. coli K-12 Using AgBr-Ag-Bi_2WO_6 nanojunction system irradiated by visible light: the role of diffusing hydroxyl radicals, *Environ.Sci. Technol*, 2010, 44, 1392-1398.

[44] K. Yu, S. Yang, C. Liu, H. Chen, H. Li, C. Sun, S. A. Boyd, Degradation of organic dyes via bismuth silver oxide initiated direct oxidation coupled with sodium bismuthate based visible light photocatalysis, *Environ. Sci. Technol*, 2012, 46, 7318-7326.

[45] S. Q. Liu, N. Zhang, Z. R. Tang, Y. J. Xu, Synthesis of one-dimensional CdS@TiO_2 core-shell nanocomposites photocatalyst for selective redox: The dual role of TiO_2 shell, *ACS Appl. Mater. Interfaces*, 2012, 4, 6378-6385.

[46] S. C. Yan, Z. S. Li, Z. G. Zou, Photodegradation of rhodamine B and methyl orange over boron-doped g-C_3N_4 under visible light irradiation, *Langmuir*, 2010, 26, 3894-3901.

[47] X. C. Wang, K. Maeda, X. F. Chen, K. Takanabe, K. Domen, Y. D. Hou, X. Z. Fu, M. Antonietti, Polymer semiconductors for artificial photosynthesis: Hydrogen evolution by mesoporous graphitic carbon nitride with visible light, *J. Am. Chem. Soc.*, 2009, 131, 1680-1681.

[48] L. Q. Ye, J. Y. Liu, C. Q. Gong, L. H. Tian, T. Y. Peng, L. Zan, Two different roles of metallic Ag on Ag/AgX/BiOX (X=Cl, Br) visible light photocatalysts: Surface plasmon resonance

and Z-scheme bridge, *ACS Catal.*, 2012, 2, 1677-1683.

[49] X. Y. Xiao, J. Jiang, L. Z. Zhang, Selective oxidation of benzyl alcohol into benzaldehyde over semiconductors under visible light: The case of $Bi_{12}O_{17}Cl_2$ nanobelts, *Appl. Catal. B.*, 2013, 142-143, 487-493.

[50] U. A. Joshi, J. R. Darwent, H. H. P. Yiu, M. J. Rosseinsky, The effect of platinum on the performance of WO_3 nanocrystal photocatalysts for the oxidation of methyl orange and iso-propanol, *J. Chem. Technol. Biotechnol*, 2011, 86, 1018-1023.

[51] M. J. Zhou, X. L. Liu, C. C. Ma, H. Q. Wang, Y. F. Tang, P. W. Huo, W. D. Shi, Y. S. Yan, J. H. Yang, Enhanced visible light photocatalytic activity of alkaline earth metal ions-doped CdSe/rGO photocatalysts synthesized by hydrothermal method, *Appl. Catal. B.*,2015, 172, 174-184.

[52] H. P. Li, J. Y. Liu, W. G. Hou, N. Duc, R. J. Zhang, X. T. Tao, Synthesis and characterization of g-C_3N_4/Bi_2MoO_6 heterojunctions with enhanced visible light photocatalytic activity, *Appl. Catal. B.*, 2014, 160-161, 89-97.

[53] L. S. Zhang, W. Z. Wang, L. Zhou, H. L. Xu, Bi_2WO_6 nano and microstructures: shape control and associated visible-light-driven photocatalytic activities, *Small*, 2007, 3, 1618-1625.

[54] D. Q. He, L. Q. Wang, H. Y. Li, T. Y. Yan, D. J. Wang, T. F. Xie, Self-assembled 3D hierarchical clew-like Bi_2WO_6 microspheres: synthesis, photo-induced charges transfer properties, and photocatalytic activities, *CrystEngComm*, 2011, 13, 4053-4059.